IOP Conf. Series: Materials Science and Engineering **257** (2017) 012012 doi:10.1088/1757-899X/257/1/012012

Finite element method analysis of cold forging for deformation and densification of Mo alloyed sintered steel

Y Kamakoshi[1, 2*], S Nishida[3], K Kanbe[2] and I Shohji[2]

[1]Dept. Applicational-Mechanical Engineering, Gunma Industrial Technology Center, Maebashi, Gunma 379-2147, Japan
[2]Division of Mechanical Science and Technology, Graduate School of Gunma University, Kiryu, Gunma 376-8515, Japan
[3]Division of Mechanical Science and Technology, Graduate School of Gunma University, Ota, Gunma 373-0057, Japan

*Corresponding author: kamakoshi-yu@pref.gunma.lg.jp

Abstract. In recent years, powder metallurgy (P/M) materials have been expected to be applied to automobile products. Then, not only high cost performance but also more strength, wear resistance, long-life and so on are required for P/M materials. As an improvement method of mechanical properties of P/M materials, a densification is expected to be one of effective processes. In this study, to examine behaviours of the densification of Mo-alloyed sintered steel in a cold-forging process, finite element method (FEM) analysis was performed. Firstly, a columnar specimen was cut out from the inner part of a sintered specimen and a load-stroke diagram was obtained by the compression test. 2D FEM analysis was performed using the obtained load-stroke diagram. To correct the errors of stress between the porous mode and the rigid-elastic mode of analysis software, the analysis of a polynominal approximation was performed. As a result, the modified true stress-true strain diagram was obtained for the sintered steel with the densification. Afterwards, 3D FEM analysis of backward extrusion was carried out using the modified true stress-true strain diagram. It was confirmed that both the shape and density of the sintered steel analyzed by new FEM analysis that we suggest correspond well with experimental ones.

1. Introduction

Mechanical parts need a stable quality, a reliable supply, a high mass-productivity and low costs. Furthermore, superior mechanical, chemical, thermal, anti-wear properties are also required for them. Wrought steel has been mainly used for automobile components. Sintered steel has been also adopted in some parts of the components. Not only requirements of more cost down for the components but also various demands for sintered steel components has been increasing in many countries year by year [1]. Compared with wrought steel, sintered steel is brittle and weak because of inner pores and microstructural defects [2]. However, it can be used as oil-less bearing utilizing porosity and as a composite material which is mixed completely different materials. Moreover, the sintered steel has superior yield rate and enables near-net-shaping, furthermore it has high form accuracy and mass-productivity of small complex shape parts. On the contrary, although the wrought steel has good mechanical properties, it is not resource saving due to high cost reprocessing. Many researchers have reported that the mechanical properties of the sintered iron materials such as tensile strength, toughness, fatigue strength, wear resistance and so on, are improved by the densification [3]. For examples, those reports are about additional elements, cold-forging and hot-forging [4], sintered cold-

forging [5], rolling of sintered ferrous alloy gear [6], powder-forged connecting rods [7] and so on. Although many studies about powder-forging with non-plastic deformation particular by methods of numerical analysis were reported [8], the numerical analysis of the sintered cold-forging with the densification and the plastic deformation was few [9]. The aim of this study is to research the behaviour of the densification of Mo-alloyed sintered steel in the cold-forging process by finite element method (FEM) analysis. Moreover, the densification and the plastic deformation of sintered steel were investigated by 3D FEM analysis.

2. Experimental Procedure

2.1. Specimen

In this study, partial diffusion alloyed steel powder (JFE steel, JIP SGM10MO-CMX) for cold-forging was prepared. It is atomized iron powder with diffusional adhered 1 mass% Mo and 0.35 mass% C (graphite powder) to the surface of powder. Then, cold-forging analysis and experiment were performed by use of sintered steel. Figure 1 shows the schematic flow of compacting and cold-forging. Steel powder was compacted to a cuboid specimen by pressure of 980 MPa (floating die method). Density (ρ_c) of the green compact was approximately 7.4 Mg/m^3. In this study, average density was measured as apparent density by the Archimedes method. Width, height and length of the cuboid specimens were 10 mm, 12 mm and 54 mm, respectively. The compacts were sintered in a vacuum furnace at vacuum degree of approximately 30 Pa. Sintering temperatures were approximately 975°C and 1050°C, and sintered time was 20 min. After sintering, density (ρ_{PS}) of the specimens were approximately 7.4 Mg/m^3. Cold-forging (CF) was performed by backward extrusion method at setting load of 1200 kN and setting time of 1 sec. In this study, only cold-forging process of the sintered specimen was simulated by FEM.

2.2. Experiment and Analysis

2.2.1. Compression test of sintered specimen. To investigate a compression load-stroke (cross head stroke of testing machine) diagram of sintered materials, the compression test was performed using an electromechanical universal testing machine (TENSILON RTF-2430 (max load: 300 kN, head speed: 1000 mm/min)). A smooth die set was used for the compression test. To reduce friction force, graphitic lubricant was used and teflon sheet was set between the die set and the specimen. Figure 2 shows the sintered specimens for the compression test. Columnar specimens (φ: 5 mm, length: 5 mm) were cut out from the inner part of the specimen. The upper columnar specimen was more densified than the lower one. The result of the compression test about the upper specimen was used as basic data for FEM analysis. The cross sectional microstructure of cold-forged specimen was observed with an inverted metallurgical microscope and the side surface of the specimen was observed with a field emission-scanning electron microscope (FE-SEM).

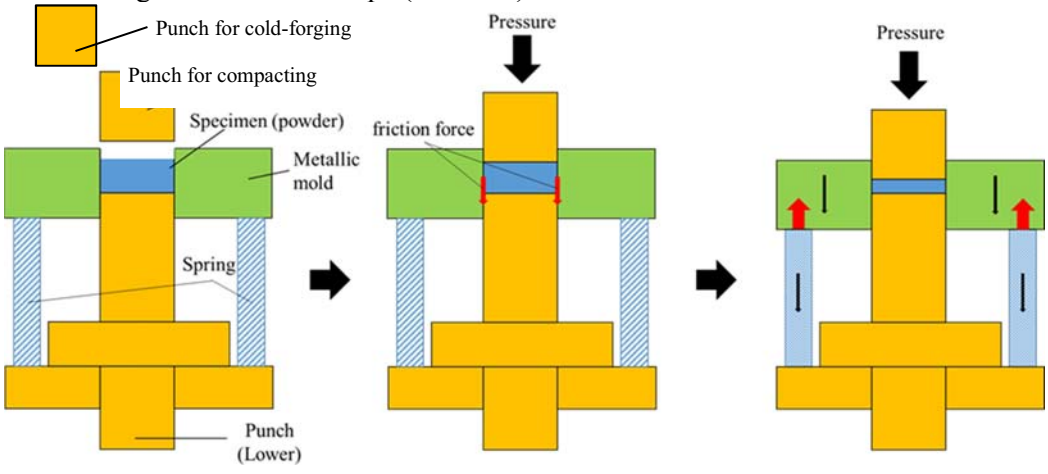

Figure 1. Schematic flow of compacting and cold-forging.
(Spring is changed to rigid-bar at cold-forging).

2.2.2. FEM analysis model. Using software "DEFORM (ver.11.0)", FEM analysis was performed to reappear a plastic flow by deformation during the cold-forging. At first, the load-stroke diagram obtained by the compression test was used for FEM analysis. Figure 3 shows the 2D analysis model for the compression test. The model was axisymmetrical one-half model and both the upper punch and the lower die were rigid material. The columnar specimen was defined as an elasto-plastic material. The 2D FEM analysis conditions are shown in table 1(1). Table 1(2)-(4) also shows the 3D FEM analysis conditions. The object type of the specimen was defined as rigid-plastic or porous. Young's modulus was 210 GPa. In case of the porous mode, initial sintered density ratio was 0.94. The mesh window was set to reduce element size of upper part of the specimen which is deformed especially. Remeshing was performed for greatly deformed area by a method of local remeshing. A normalized Cockroft & Latham model was used as the fracture model. In the model, a damage value (critical value) and the fracture element were 100 and 1, respectively. Then the load-stroke diagram obtained by 2D FEM analysis was used for 3D FEM.

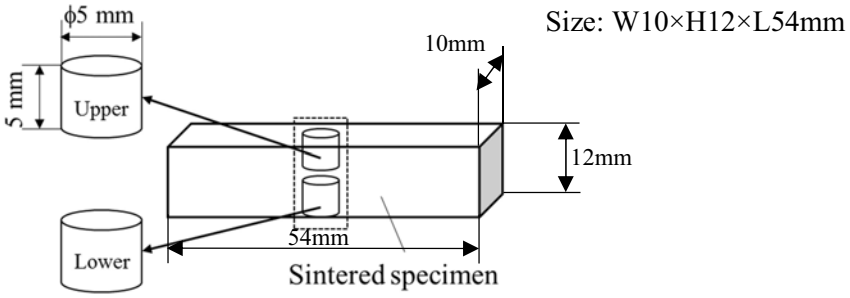

Figure 2. Specimens for compression test.

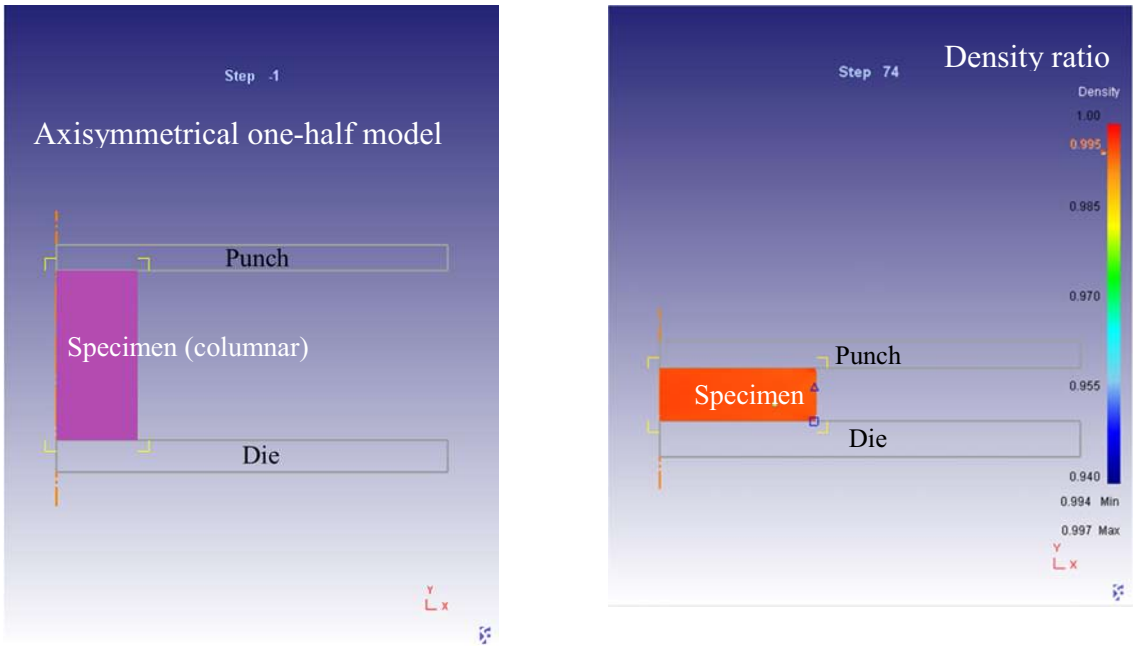

(a) Layout of punch, specimen and die before compression test.

(b) Example of analysis result after compression test.

Figure 3. 2D analysis model for compression test.

Table 1. FEM analysis conditions for cold-forging of sintered material.

Object Type/ Model/ Method	(1) Elasto-plastic material/ Axisymmetric 2D model	(2) Rigid-plastic material/ 3D model	(3) Porous material/ 3D model/ remeshing	(4) Porous material/ 3D model/ remeshing and element elimination method
Density (relative density)	–	–	0.94	0.94
Element count [count]	2,103	158,389	148,148	148,148
Calculation step [step]	90	500	2000	2000
Punch speed [mm/sec]	16.667	1	1	1
Step increment [mm/step] (die displacement)	0.05	0.01	0.001	0.001
Shear friction coefficient between a specimen and a punch	0.01	0.4	0.4	0.4
Shear friction coefficient between a specimen and a die	0.01	0.08	0.08	0.08
Remeshing [mm] (Maximum stroke increment)	–	–	0.01	0.01
Target volume (for meshing)	–	–	Valid	Valid
Cockroft & Latham marginal damage value	–	–	–	100
Fracture element	–	–	–	1

Table 2. Result of density measurement after compression test.

Specimen	Sintering temperature [°C]	Cut position	Density before compression test [Mg/m^3]	Density after compression test [Mg/m^3]	Density ratio [%]*
A	975	Upper	7.4	7.76	98.5
B	1050			7.80	99.1
A	975	Lower	7.4	7.70	97.8
B	1050			7.72	98.0

* Density of wrought steel is defined as 7.874 Mg/m^3.

Table 3. Comparison in size of specimens before and after compression test

Specimen	Sintering temperature [°C]	Cut position	Radius [mm] (before)	Radius [mm] (after)	Height [mm] (before)	Height [mm] (after)	Compression ratio [%] (using height)
A	975°C	Upper	5.0	9.6	4.90	1.27	74.1
B	1050°C		5.0	9.0	5.22	1.54	70.6
A	975°C	Lower	5.0	8.3	5.22	1.83	65.0
B	1050°C		5.0	8.8	5.49	1.72	68.7

3. Results and Discussion

3.1. Properties and microstructure of specimen after compression test

Table 2 shows density change of the columnar specimen by the compression test. Density ratios were above 98.5% or equals at the upper part of the specimen. These results mean that the sintered specimen has high-deformational properties. Table 3 shows size change of the specimens before and after the compression test. Compression ratios were above 70% at the upper part of the specimens. The upper part was slightly more densified than the lower part because of its contacting the upper punch and one-way press at the cold-forging. Figure 4 shows a side surface area and a cross section at the upper part of cut specimen-B after the compression test. No crack was observed in both the cross

section and the side surface area. Figure 4(c) shows that the upper part of the cut specimen-B was successfully compressed with the plastic flow. These results mean that the sintered specimen has a compressibility which is nearly equivalent to the wrought steel.

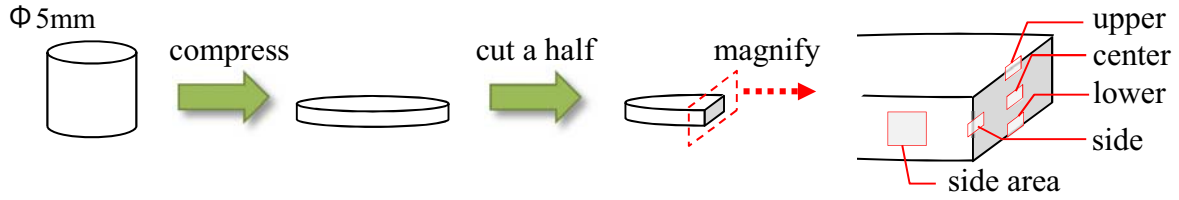

(a) Observed area of specimen

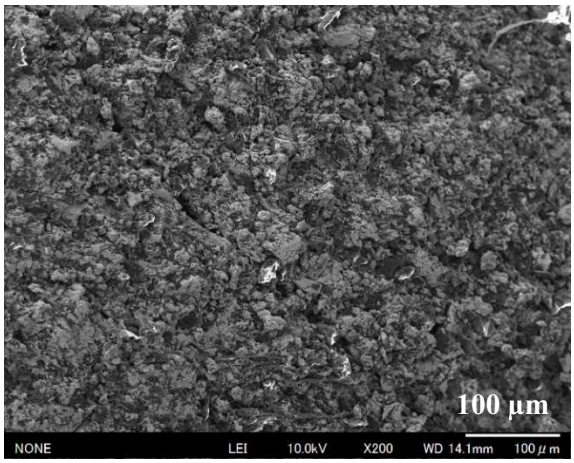

(b) SEM image of surface of side area

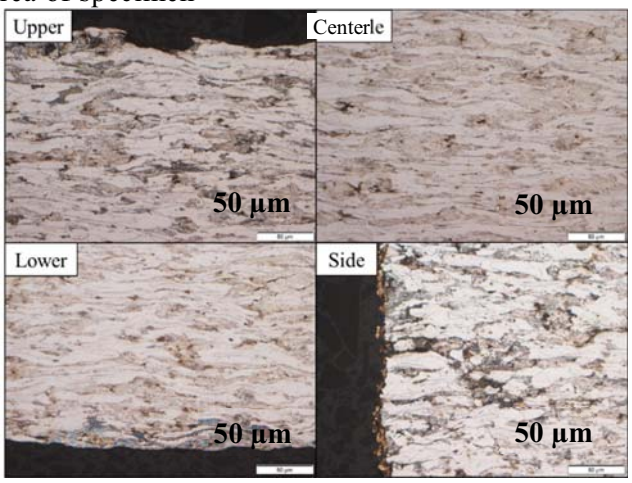

(c) OM images of cross section

Figure 4. Surface of side area and cross section of specimen-B after compression test.

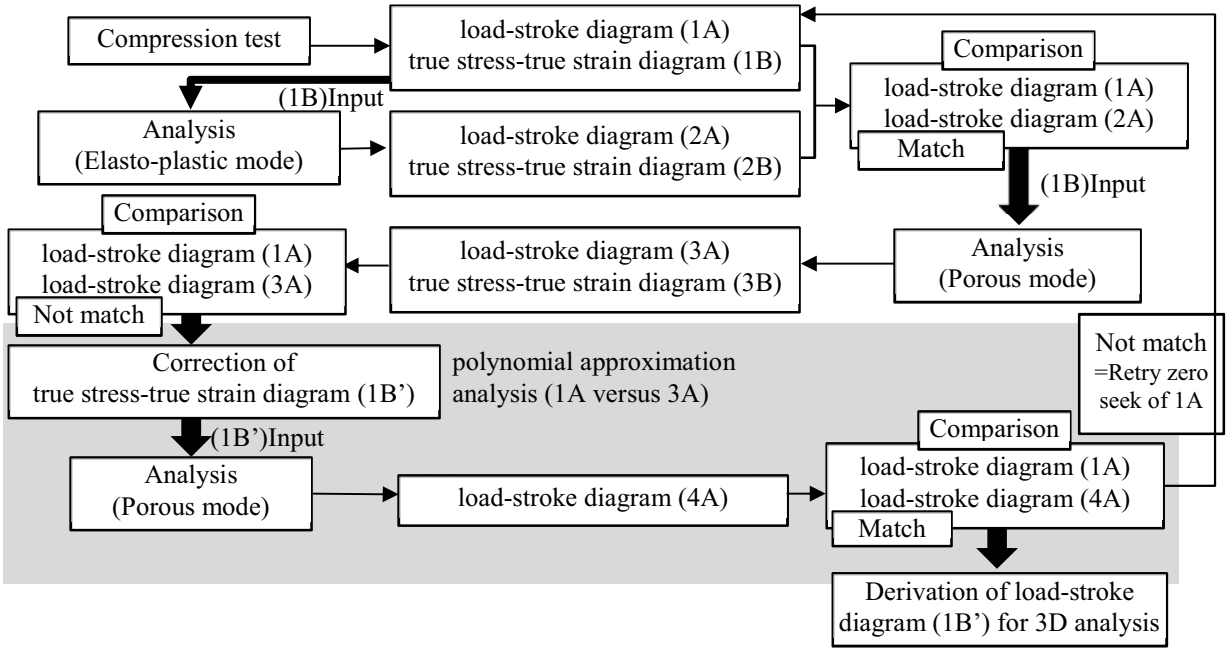

Figure 5. 2D deformation analysis procedure for sintered material.

3.2. Derivation of load-stroke diagram for sintered material by 2D deformation analysis

Since this subsection, the data of the specimen-B are used. Figure 5 shows process of 2D analysis. Suffixes A and B of diagram number shown in the figure mean load-stroke and true stress-true strain,

respectively. At first, load-stroke diagram (1A) was obtained by the compression test of the columnar specimen. The diagram (1A) was corrected by zero seek and changed a nominal stress-nominal strain diagram.

Table 4. Comparison in compression amount and density ratio for experiment and analysis values.

	Compression amount [mm]	Density ratio [-]	Error in density ratio [%]
Experiment	3.68	0.991	-
Analysis	3.70	0.995	0.4

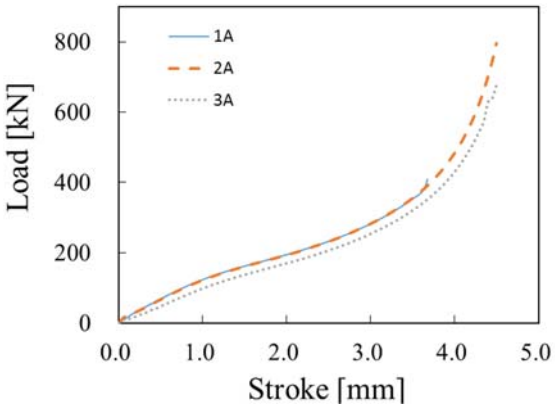

(a) Load-stroke diagrams (1A, 2A, 3A).

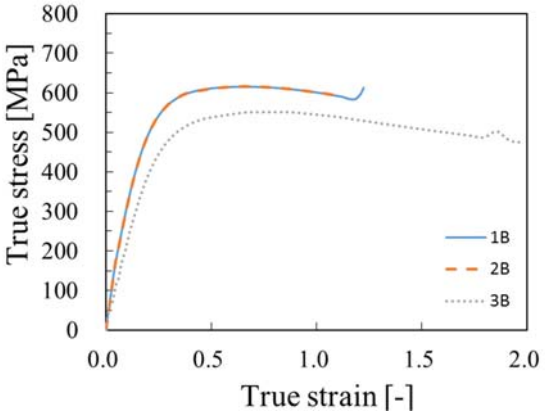

(b) True stress-true strain diagrams (1B, 2B, 3B).

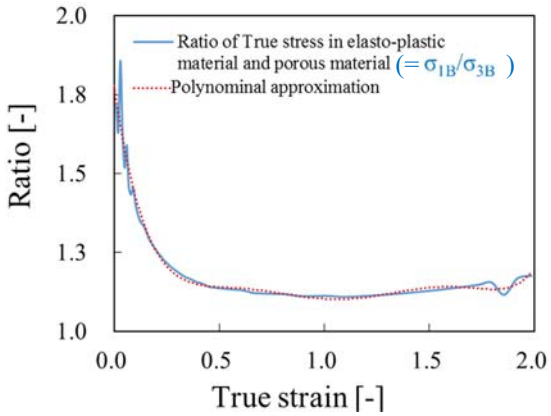

(c) Ratio of true stress in elasto-plastic material and porous material.

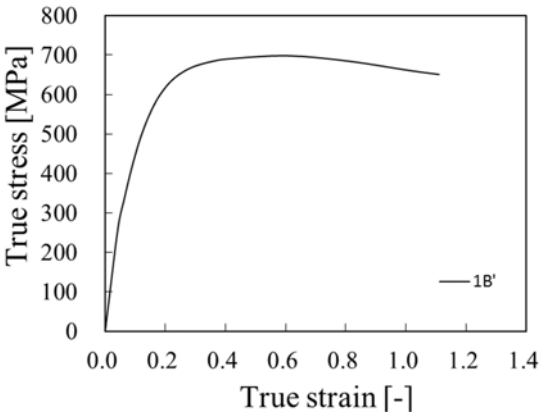

(d) Corrected true stress-true strain diagram (1B'). (1B'=1B × ratio of true stress).

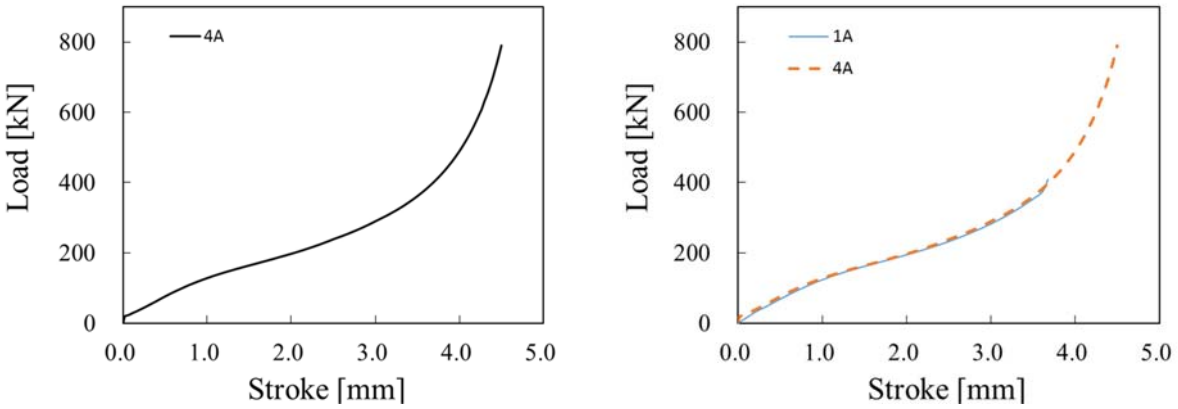

(e) Load-stroke diagram (4A). **(f)** Comparison of load-stroke diagrams (1A, 4A)

Figure 6. Results of 2D deformation analysis used axisymmetrical columnar model.

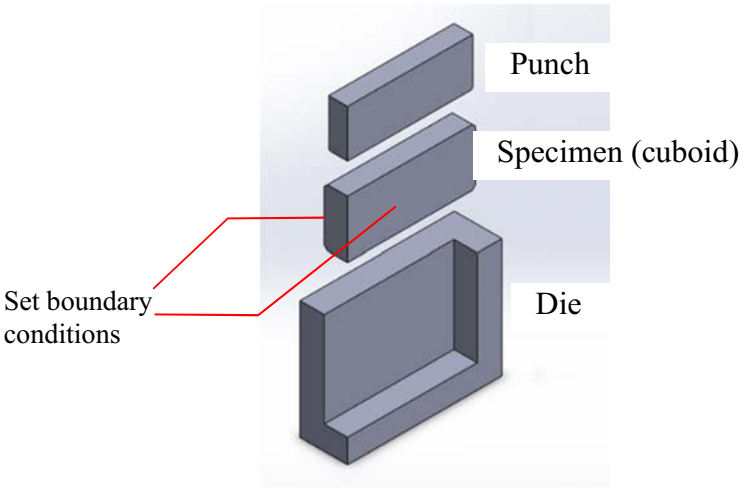

Figure 7. 1/4 model for 3D FEM analysis in cold-forging.

It was converted to a true stress-true strain diagram (1B). Using the true stress-true strain diagram (1B), the compression test was analyzed by the elasto-plastic material mode. Then a load-stroke diagram (2A) and a true stress-true strain diagram (2B) were obtained. When compared with the load-stroke diagrams (1A) and (2A), match of both diagrams was confirmed. Next, the compression test was analyzed with the porous material mode using the true stress-true strain diagram (1B). As a result, a load-stroke diagram (3A) was obtained. When compared with the load-stroke diagrams (1A) and (3A), both diagrams did not correspond constantly. The reason seems that the analysis result was performed with the porous material mode although the data of the diagram (1A) already involved compression property of the porous. Therefore, to correct difference of both diagrams (1A) and (3A), a polynomial approximation analysis was used anew. Processes are as follows.

(i) Check what times load of diagram (1A) is that of diagram (3A) at the same stroke value.

(ii) To obtain amplification coefficient in the true stress-true strain diagram, the polynominal approximation is performed. In this study, the polynominal of sixth degree (shown in figure 6(c)) is used.

(iii) Multiply the obtained amplification coefficients by the true stress in the true stress-true strain diagram (1B). Then the modified true stresses of diagram (1B') is obtained.

(iv) Analyze the compression test with the porous material mode using the diagram (1B') and obtain diagram (4A).

As a result, the load-stroke diagram (4A) matched load-stroke diagram (1A). Therefore, the modified diagram (1B') was used for 3D deformation analysis after this. Figure 6 shows all of

diagrams which were obtained according to above mentioned procedure. Table 4 shows results of comparing in compression amount and density ratio. The results indicated that analysis values were quite close to experimental values for the compression amount and the density ratio. Also the results indicated that 2D analysis model in above procedure is proper in this study.

3.3. 3D deformation analysis of porous material

3.3.1. Analysis model. Figure 7 shows the 3D FEM model for the compression test. Considering the symmetry, the 1/4 model was used. The cuboid specimen was inserted into the die and compressed by the upper punch. The area of the die inserted the specimen and that of the upper punch were 10×55 mm and 8×53 mm, respectively. Then, after cold-forging, the flash (equals to rim) width by deformation was almost 1mm.

3.3.2. Results of analysis and improvement of analysis method. Figure 8 and 9 show comparison of equivalent strain distribution in rigid-plastic material model and porous material model analyzed under conditions of table 1(2) and (3), respectively. In case of rigid-plastic material model, the punch load was saturated at approximately 1000 kN. On the other hand, in case of porous material model, equivalent strain of the corner part increased to 28.7 and the punch load increased to above 1800 kN. Since the real load of the upper punch which was measured by a strain gauge was approximately 800 kN, the result is invalid. To improve the analysis method, the forced remeshing mode was selected. In this mode, when maximum stroke increment reaches to 0.01 mm in the specimen, remeshing is performed to the elements in the upper parts at 4 mm height. The target volume mode which hold volume constantly by interpolation is also used to avoid volume reduction at calculation and remeshing. The target volume mode is only valid in remeshing. As shown in figure 8 and 9, the height of flash in the porous material model is lower than that of the rigid-plastic material model. This phenomenon indicates that volume reduction occurs by not only microstructure deformation but also reducing pores at the compression test. Thus, to avoid increasing strain locally, analysis with the element elimination method is effective. In particular, this method is valid for the porous material model that strain concentration occurs easily by volume reduction. With increasing density of the sintered material, the properties of plastic deformation approaches those of the rigid-plastic material. In this case, local strain concentration is unnatural. In this study, when the damage value of the element greatly exceeds those of surrounding elements, the element is vanished. The damage value was determined using the normalized Cockroft and Latham equation. The marginal damage value was selected 100. Figure 10 shows the analysis result using the porous material model, the modified true stress-true strain diagram (1B'), and the remeshing and element elimination method under conditions of table 1(4). In figure 10 (a), a example photo of the cold-forged specimen is also shown. The shape of the analyzed specimen almost corresponds to that of the cold-forged specimen.

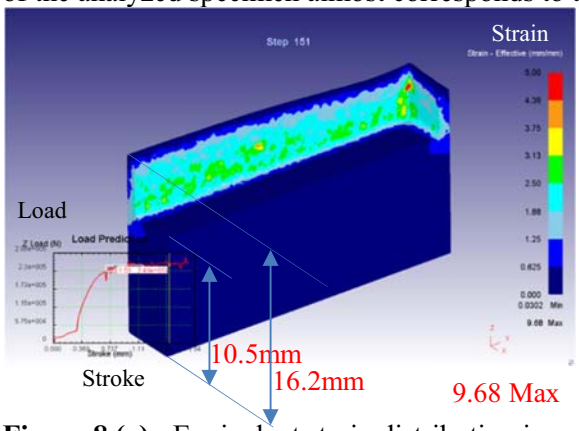

Figure 8 (a). Equivalent strain distribution in rigid-plastic material model analyzed under conditions of table 1(2).

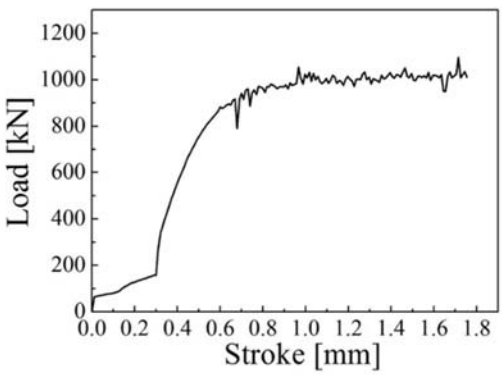

Figure 8 (b). Magnified graph of load-stroke diagram in figure 8 (a).

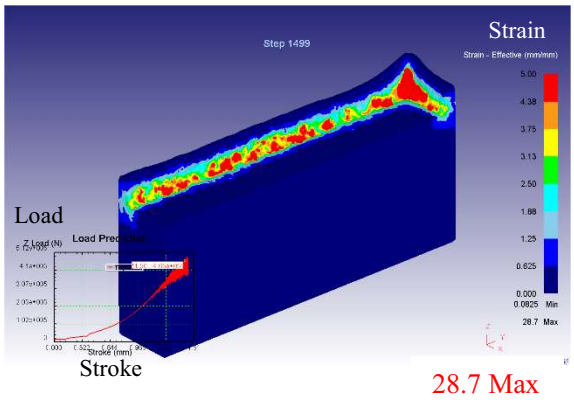

Figure 9 (a). Equivalent strain distribution in porous material model analyzed under conditions of table 1(3).

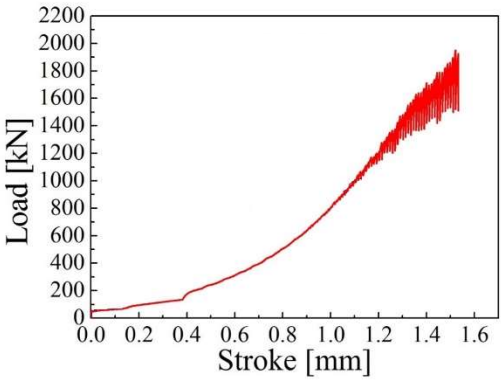

Figure 9 (b). Magnified graph of load-stroke diagram in Fig. 9a.

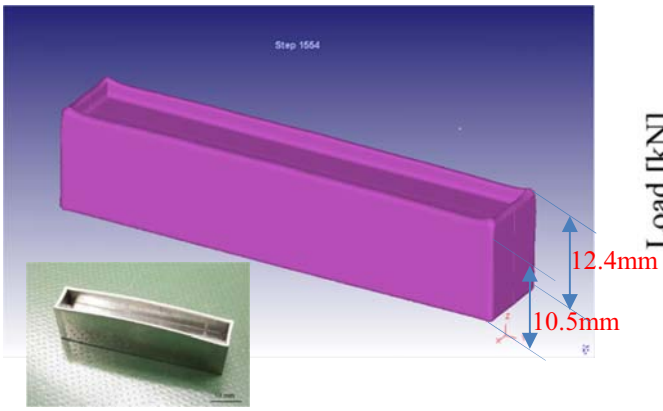

Example photo of cold-forged specimen

Figure 10 (a). Analysis result using remeshing and element elimination method for cold-forged specimen under conditions of table 1(4).

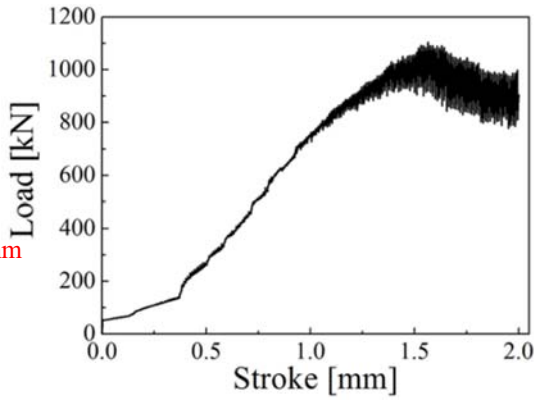

Figure 10 (b). Load-stroke diagram obtained by FEM analysis using remeshing and element elimination method in cold-forging.

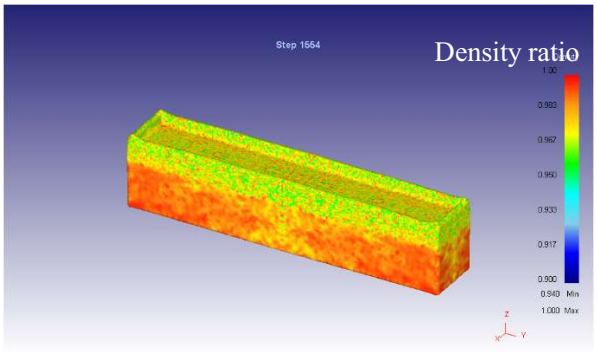

Figure 11 (a). Density distribution by cold forging analyzed using element elimination method (specimen-B, sintering temperature: 1050°C).

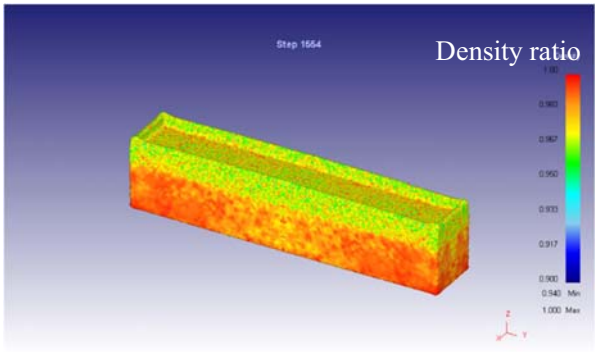

Figure 11 (b). Density distribution by cold forging analyzed using element elimination method (specimen-A, sintering temperature: 975°C).

Table 5. Comparison of experiment and 3D analysis values. ( ) : Error for experimental value[%]

	Specimen-B (sintering at 1050°C)		Specimen-A (sintering at 975°C)	
	Density ratio [-]	Flash height [mm]	Density ratio [-]	Flash height [mm]
Experiment	0.991	2.03	0.990	2.05
Analysis	0.978 (1.3%)	1.95 (3.9%)	0.978 (1.2%)	1.98 (3.4%)

As shown in Fig.10b, the load-stroke diagram in the cold-forging process can be obtained by FEM analysis and the load greatly fluctuates at the stroke above 1.0 mm. The fluctuation is caused by the remeshing. Fig. 8 shows the analysis result in case of the punch stroke 1.55 mm by rigid-plastic material model. The height from the bottom surface to the upper surface in the center was 10.5 mm and the maximum height of flash was 16.2 mm. In case of porous material model, both heights were 10.5 mm and 12.4 mm, respectively (Fig. 10a). These values approximately corresponded to sizes of real sintered cold-forged specimens (ρ_{CF}: 7.8 Mg/m^3, PS: 1000°C, 20 min). The shape of flash was similar to that of the real sintered cold-forged specimen and gradually increased from the edge to the center part. The fluctuation in the load in Fig. 10b is smaller than that in Fig. 9b and saturates at approximately 1000 kN. The results mean that the remeshing and element elimination method is effective to simulate cold-forging process. The load-stroke diagram in Fig. 10 is relatively similar to that in Fig. 8 and more reliable than the result in Fig. 9. Fig. 11 shows density distribution of the specimen which was analyzed by using the element elimination method. Table 5 shows comparison of experimental and 3D analysis values for the density ratio and the flash height. As shown in table 5, regardless of sintering temperature (1050°C and 975°C), the averages of the density ratios of the real sintered cold-forged specimens were approximately 0.99 and those evaluated by FEM analysis were approximately 0.978. As for the flash height, the error for the experimental value of the specimen-B and A are 3.9% and 3.4%, respectively. These analysis results almost corresponded with those of the real sintered cold-forged specimens. Therefore, the analysis model suggested in this study would be applicable to simulate the densification of the sintered iron products.

4. Conclusions

To examine behaviours of the densification of Mo-alloyed sintered steel in the cold-forging process, the plastic deformation properties of the sintered steel were investigated by 3D FEM analysis. The suggested 3D analysis method enables to express the properties of the densification and the plastic deformation of the sintered cold-forged specimen. At first, the true stress-true strain diagram was obtained from the compression test. In the next, to determine the modified true stress-true strain diagram for 3D FEM analysis, the analysis of polynomial approximation was performed by use of analytical and experimental load-stroke diagrams. Using the modified true stress-true strain diagram, the analysis of backward extrusion was carried out. As a result, it was confirmed that the shape and the density of the sintered steel analyzed by 3D FEM correspond well with the actual values. Thus, validity of the analysis model for the sintered cold-forged steel was indicated. The analysis model suggested in this study would be applicable to simulate the local densification for the sintered steel parts.

Acknowledgements

The authors express their sincere gratitude to Y Morokuma (Gunma University), R Abe (Fuji Sintering Alloy Co., Ltd.), and T Suganuma (Chubureikan Co., Ltd.).

References

[1] K S Narasimhan 2007 Technology advances for the growth of powder metal in automotive applications *Japan Society of Powder and Powder Metallurgy* **54** 499-505
[2] O Yukiko, O Tomoshige, T Tsuguyuki, U Satoshi 2011 Effects of Apparent Density on Compacting Behavior of Atomized Iron Powder, *Japan Society of Powder and Powder Metallurgy* **58** 83-90

[3] M Kondoh 2007 Development of High Accuracy, High Density Powder Compaction Technology, *Japan Society of Powder and Powder Metallurgy* **54** 506-512
[4] Kandavel T K, Chandramouli R, Shanmugasundaram D 2009 Experimental study of the plastic deformation and densification behaviour of some sintered low alloy P/M steels, *Materials & Design* **30** 1768-1776
[5] N Nakamura, S Uenosono, M Fujinaga, S Koizumi, H Anma, T Yoshimura 2005 Sintering and Cold-Forging Process for High Density Sintered Materials, *JFE GIHO* **7** 19-23
[6] S Unami, T Goushi, K Kudo, F Tsumori, H Kang and H Miura 2011 Implovement of Surface Densification and Fatigue Strength by Tooth Root Rolling of Sintered Ferrous Alloy Gear Added Mo, *J.Jpn.Soc.Powder and Powder Metallurgy* **58** 692-696
[7] K Takada, R Kogure, T Kobayashi 2007 Research of High Fatigue Strength for Powder-Forged Connecting Rods, *Honda R&D Technical Review* **19** 129-137
[8] S Yi, L Yuan-yuan, Z Zhao-yao, Z Zhen-xing, C Pu-quing 2010 Improved model and 3D simulation of densification process for iron powder, *Transactions of Nonferrous Metals Society of China* **20** 1470-1475
[9] T Nagata, T Takemasu, T Koide and S Nishida 2016 Bending Durability of Ni-Mo pre-alloyed Sintered Steel Case-Carburizing Gears with Different Densities and Tooth Root Bending Stress Analysis Using FEM Model Considering Voids, *Japan Society of Powder and Powder Metallurgy* **63** 17-22